

# Ferroelectricity of Li-doped silver niobate (Ag,Li)NbO<sub>3</sub>

Desheng Fu<sup>1</sup>, Makoto Endo<sup>2</sup>, Hiroki Taniguchi<sup>2</sup>,  
Tomoyasu Taniyama<sup>2</sup>, Mitsuru Itoh<sup>2</sup>, and Shin-ya Koshihara<sup>3,4</sup>

<sup>1</sup>Division of Global Research Leaders, Shizuoka University,  
Johoku 3-5-1, Naka-ku, Hamamatsu 432-8561, Japan

<sup>2</sup>Materials and Structures Laboratory, Tokyo Institute of Technology,  
4259 Nagatsuta, Yokohama 226-8503, Japan

<sup>3</sup>Department of Materials Science, Tokyo Institute of Technology,  
Meguro-ku, Tokyo 152-8551, Japan

<sup>4</sup>CREST & ERATO, Japan Science and Technology Agency (JST),  
3-5 Sanbanchou, Chiyoda-ku, Tokyo 102-0075, Japan

E-mail: ddsfu@ipc.shizuoka.ac.jp

January 12, 2013

## Abstract

Phase evolution in (Ag<sub>1-x</sub>Li<sub>x</sub>)NbO<sub>3</sub> (ALN) solid solution was investigated by X-ray diffraction technique, dielectric and polarization measurements. It is shown that small substitution of Ag with Li gives rise to an orthorhombic-rhombohedral structural transformation in ABO<sub>3</sub>-perovskite silver niobate at room temperature. Structural refinements indicate that both A- and B-site displacements contribute to the spontaneous polarization of the ferroelectric phase with symmetry *R3c*. Increasing Li-concentration enhances the ferroelectric rhombohedral distortion, resulting in the increase of the para-ferroelectric phase transition temperature and the polarization of the solid solutions.

# 1 Introduction

Ferroelectric materials, which have high dielectric constant and large spontaneous polarization, offer various applications ranging from electronic devices, telecommunication, medical imaging and ultrasonic devices, to ferroelectric memories [1, 2, 3]. The prototype ferroelectrics include  $\text{BaTiO}_3$  and  $\text{PbTiO}_3$ : the former is generally used for the fabrication of the capacitive devices while the latter is a base material for the piezoelectric devices. For  $\text{BaTiO}_3$ , the problems that hamper its technological applications are the discontinuity of physical properties around room temperature due to a structural phase transition and the relatively-low ferroelectric phase transition  $T_c^{\text{FE}}$  ( $\sim 400\text{K}$ ) [4]. On the other hand,  $\text{PbTiO}_3$ -based materials show high  $T_c^{\text{FE}}$  and high dielectric/piezoelectric responses, but contain hazardous lead, which raises a serious environmental concern[5]. Currently, increasing effort is being made to develop lead-free ferroelectric materials with high  $T_c^{\text{FE}}$  and high performances of physical properties [5, 6, 7, 8, 9, 10].

Ferroelectricity in the  $\text{ABO}_3$ -perovskites is basically driven by the cooperative displacement of B-site atoms filling the octahedral site. Modern investigations further reveal that the strong hybridization between metal atom and oxygen is essential for the origin of ferroelectricity in these perovskite oxides [11]. In contrast to  $\text{BaTiO}_3$  in which polarization is originated from the B-site atomic displacement, the lead-based materials generally show large A-site atomic displacement in the dodecahedral cave in addition to the B-site atomic displacements[12]. It is considered that the strong covalency of Pb-O effectively softens the short-range repulsive interaction between atoms and favors Pb to move into an off-centering position in the perovskite structure of the lead compounds.[11, 13] It is generally accepted that such hybridization characteristic is crucial for the high piezoelectric performance of the lead-based materials. Apparently, it also outlines a basic direction toward searching novel element to replace the hazardous Pb in the perovskite oxides. Ag seems to be a promising candidate because it has been shown theoretically that Ag has a strong hybridization with oxygen in the perovskite compounds [10, 14, 15]. From the recent structural data [16], we can evaluate the bond lengths of Ag-O in  $\text{AgNbO}_3$ , and find that the shortest bond length of Ag-O is indeed significantly less than the sum of silver and oxygen ionic radii, supporting the theoretical prediction of the strong covalent bonding in silver perovskites. It is naturally expected that A-site driven polarization may be realized in the silver perovskites. Actually, experimental investigations reveal

that a ferroelectric state with exceptionally high polarization ( $52 \mu\text{C}/\text{cm}^2$  for polycrystal sample) can be induced in  $\text{AgNbO}_3$  through the application of a high electric field.[17] Thus both theoretical and experimental findings suggest that Ag possesses the essential features of Pb to cause a strong ferroelectric distortion in the niobate perovskite, and good ferroelectrics are highly expected in the silver perovskites.

In addition to the application of a high electric field, preliminary investigations indicate that small substitution of Ag with K or Li can change the structure of  $\text{AgNbO}_3$ , in which oxygen octahedral tilting due to the low tolerance factor[16, 18] occurs and hampers the ferroelectric distortion, into a ferroelectric structure with large polarization and piezoelectric response[19, 20]. Currently, there is rather large disagreement in literature about the crystal structure of  $\text{AgNbO}_3$ . [21, 22, 23] Also, the reports on the structure of its solid solutions are very limited and sometime confused. [24, 25, 26]. The origin of its ferroelectricity is still lack of understanding. In this study, we carried out a systematical investigation on the effects of Li substitution on the ferroelectricity of  $\text{AgNbO}_3$ . We show that the evolution of ferroelectricity is closely related to the rhombohedral distortion caused by the Li-substitution. The present investigations may improve our understanding of the ferroelectricity in the silver-based perovskites.

## 2 Experimental

$\text{Ag}_{1-x}\text{Li}_x\text{NbO}_3$  (ALN) polycrystals were prepared by a solid state reaction approach. Appropriate amounts with stoichiometric ratio of  $\text{Ag}_2\text{O}$ ,  $\text{Nb}_2\text{O}_5$ , and  $\text{Li}_2\text{CO}_3$  were mixed homogeneously with ethanol and calcined at 1253 K for 6 hours in  $\text{O}_2$  atmosphere, followed by removing the powder out of the furnace to allow a rapid cooling for preventing the phase separation. The calcined powder was milled again and pressed to form pellets that were sintered at 1323 K for 6 hours in  $\text{O}_2$  atmosphere, followed by a rapid cooling. Single crystal samples were obtained from the calcined powder by a melt growth process described in a previous report[19].

X-ray diffraction technique was used to determine the structure and lattice parameters of ALN solid solutions. For electrical measurements, the sintered pellets were polished and coated with the Au electrodes. Dielectric measurements were performed in a temperature range of 300 K  $\sim$  850 K by using a Hewlett-Packard Precision LCR meter (HP4284A) at an ac level of

1V/mm. Dielectric ( $D - E$ ) loops were measured at room temperature with a ferroelectric measurement system of aixACCT TF Analyzer 2000 equipped with a high voltage source of 10 kV. To prevent air breakdown at the high field, samples were immersed in silicon oil during the measurements.

Inductively coupled plasma (ICP) spectrometry (HORIBA-JOBIN-YVON ULTIMA2) was used to determine the chemical composition of samples with an error less than 0.2 mol%. To prepare the solution for ICP measurements, 2 mg of the same sample used for electrical measurements was mixed with 10 ml sulfuric acid and 2g ammonium sulfate, and dissolved at 503 K for 20 minutes with autoclave. ICP analysis indicates that the deviation of Li concentration from the starting material for ceramics samples is less than 1%, while relatively-large deviation is observed for the single crystals.

## 3 Results and Discussions

### 3.1 X-ray diffraction patterns

Figure 1 shows the X-ray diffraction patterns observed at room temperature for several compositions of ALN powders. It is immediately clear that there is a structural transformation as incorporating Li into Ag site. The phase boundary is found to locate at composition of  $x_c \approx 0.05 - 0.06$ . For  $x < x_c$ , the solid solution possesses the orthorhombic structure of pure  $\text{AgNbO}_3$  [18, 24]. When  $x$  is larger than  $x_c$ , however, the solid solution transforms into a rhombohedral structure[24]. Such rhombohedral symmetry can be unambiguously seen from the splittings of 200, 220, 222 pseudocubic reflections and supported from structural refinements described in the next section. This rhombohedral phase remains unchanged for composition  $x < \sim 0.12$ . However, further increase in Li-concentration will lead to the occurrence of second phase of  $\text{LiNbO}_3$  hexagonal pseudo-ilmenite-type.

### 3.2 Structural refinements of the rhombohedral phase

The detailed structure of pure  $\text{AgNbO}_3$  has been investigated by various techniques including x-ray and neutron diffractions[16, 21]. These structural analyses predict centrosymmetric  $Pbcm$  space group for the room temperature phase. It should be pointed out that such centrosymmetric space group is inconsistent with the experimental results from dielectric, polariza-

tion and piezoelectric measurements[6, 27], which indicate the existence of weak ferroelectricity in  $\text{AgNbO}_3$  at room temperature. Such discrepancy is very likely due to the extremely-small atom displacement in the structure, resulting in the difficulty of its detection by X-ray or neutron diffractions. Actually, the reported X-ray or neutron diffraction analyses could not distinguish between centrosymmetric  $Pbcm$  and noncentrosymmetric  $Pbc2_1$  space groups[16]. The exact determination of the space group of  $\text{AgNbO}_3$  room temperature phase goes beyond the scope of present investigation, and remains to be addressed in future work.

On the other hand, there is still a lack of knowledge of the detailed structure of the ALN rhombohedral phase. In order to gain an insight into the ferroelectricity of this material, we then carried out a preliminary analysis on the structure of the ALN rhombohedral phase. To achieve such a purpose, we collected powder X-ray diffraction data in the  $2\theta$  range of  $20^\circ - 130^\circ$  at a step width of  $0.01^\circ$  by using Bruker AXS D8 ADVANCE powder diffractometer (X-ray source is the radiation of  $\text{Cu } K\alpha$ ). Measurements were performed at room temperature with a powder sample of  $x = 0.10$ . An intensity of about  $6 \times 10^5$  counts was measured for the strongest diffraction peak around  $2\theta \sim 32.2^\circ$ . The structural refinements were then performed using the Rietveld refinement program X'Pert Plus. A pseudo-Voigt profile function was used and the ratio of  $K\alpha_2$  and  $K\alpha_1$  was assumed as 0.5 during the refinements. We obtained refinements with reasonably-good  $R$ -factors for the space group  $R3c$ . Figure 2 shows the results of the refinements. The fit between the observed and calculated profiles is quite satisfactory. Table 1 lists the structural parameters for this phase model. From this structure, we can see that this rhombohedral  $R3c$  phase involves polar displacements of the Ag/Li, Nb, and O atoms along the pseudocubic  $[111]$  direction. This is also supported by the spontaneous polarization measurements[19], which show that the polarization along  $[111]$  direction is larger than that along  $[001]$  direction. This structural model supports our inference that incorporation of Li into the Ag site favors the rhombohedral ferroelectric distortion over the oxygen octahedral tilting in the perovskite structure.

### 3.3 Dielectric properties

The phase transformation observed by X-ray diffraction technique is also confirmed in the dielectric measurements(Fig. 3). For  $x < x_c$ , ALN exhibits the dielectric behaviors similar to that of pure  $\text{AgNbO}_3$ [17], indicating the

same phase transition sequences between them. Similar to  $\text{AgNbO}_3$ , there are four detectable anomalies of dielectric constant ( $\epsilon'$ ) in the ALN solid solutions upon heating. For  $\text{AgNbO}_3$ , the cusp at  $\sim 340$  K is interpreted to the disappearance of weak ferroelectricity [27]. Following the cusp at  $\sim 340$  K, there is a broad peak at  $\sim 540$  K. It is suggested to be related to the dynamics of antiparallel Nb displacements [28], however, its origin remained to be clarified. A sharp jump at 624 K can be well explained by an antiferroelectric phase transition [16, 18, 22]. A turning point following the antiferroelectric phase transition can be seen at 668 K and is basically caused by oxygen octahedral tilting transition [16]. Generally, the variation in dielectric response is small at transition point associating with the oxygen octahedral tilting transition.

In sharp contrast to composition with  $x < x_c$ , ALN solid solution with  $x > x_c$  shows different temperature behaviors of the dielectric constant. A Curie-Weiss-type ferroelectric phase transition occurs at  $T = T_c^{\text{FE}}$ , and  $T_c^{\text{FE}}$  increases with the increase of the Li-concentration. Curie-Weiss constant is evaluated to be  $C = 5.4 \cdot 10^5$  K for  $x = 0.119$ . There is another dielectric anomaly after the ferroelectric phase transition. Polarization measurements indicate that this is a nonpolar phase. X-ray diffraction measurements by Sakabe et al.[25] suggest that it is belong to monoclinic phase. Apparently, further works are necessary to understand structural change occurring in the high temperature range.

### 3.4 Spontaneous polarization

In order to observe the evolution of the ferroelectricity in the ALN solid solutions, we also carried out measurements on  $D - E$  loops for the ceramics samples and two single crystals with  $(001)_c$  crystal face at room temperature. The results are summarized in Fig.4. For pure  $\text{AgNbO}_3$ , only slim loop can be observed when electric field is lower than 110 kv/cm, but double hysteresis loops with extremely-large polarization can be clearly seen at higher field[17]. Around the phase boundary, the double hysteresis loop changes into a normal ferroelectric loop, clearly indicating that the incorporation of Li into the Ag-site effectively unlocks the strong local polarization in  $\text{AgNbO}_3$ . The remanent polarization  $P_r$  measured at 80 kV/cm for ALN ceramics are given in Fig. 4(c). Again, we can see a sharp jump of  $P_r$  at phase boundary, indicating that a ferroelectric state with large polarization is established in the rhombohedral phase. All ceramics samples show  $P_r$  value comparable

to that of BaTiO<sub>3</sub> single crystal (26  $\mu\text{C}/\text{cm}^2$ ) [29]. Moreover, the polarization in ALN solid solution is very stable after switching. This is evident from the ideal square shape of the loop. Large  $P_r$  value and ideal bistable polarization state of ALN ceramics may be interesting for the non-volatile ferroelectric memory applications because memory devices constructed generally from PZT or Bi-layer-structure ferroelectrics suffer the poor retention of stored information or degradation of performance due to the polarization destabilization or rather small remanent polarization [30].

Although we observed a slight decrease in  $P_r$  with Li concentration ( $x > x_c$ ) in ceramics samples, it can be reasonably accounted for in terms of an insufficient poling field. As shown in inset of Fig. 4(a), a saturation value of  $P_r$  is not available for the sample of  $x = 0.091$  at the present applied field. Obviously, higher electric field are necessary to obtain a saturation state.

In order to examine the effect of Li-substitution on spontaneous polarization, single crystals with natural facet of pseudocubic (001)<sub>c</sub> were then used to obtain the  $D-E$  loops. Fig. 4(b) shows that Li-substitution enhances the spontaneous polarization of ALN with the rhombohedral structure. Because the polar axis is along  $\langle 111 \rangle_c$  in the rhombohedral phase as described above and shown in Ref.[19], the spontaneous polarization is then estimated from the relationship  $P_s = \sqrt{3}P_s^{<001>}$ , and is found to increase with increasing Li-concentration as shown in Fig. 4(c).

## 4 Discussion

### 4.1 Relationship between ferroelectricity and rhombohedral distortion

In a recent *ab initio* study of AgNbO<sub>3</sub>, it is shown that Ag has a large displacement (0.50 Å) than that (0.22 Å) of Nb in a tetragonal structure[10, 14], indicating that Ag has a strong ability to shift to an off-centering position in AgNbO<sub>3</sub>. It seems that the weak ferroelectricity and strong antiferroelectricity in AgNbO<sub>3</sub> may be reasonably attributed to Nb and Ag displacements respectively[17]. When Li is introduced into Ag site, the volume of perovskite cell will decrease with Li-concentration due to the small ionic radius of Li<sup>+</sup> (0.92 Å) with respect to Ag<sup>+</sup> (1.28 Å). Fig. 5(c) really shows such variation in the cell volume. Apparently, suppression of unit cell will reduce the space available for atomic displacements in the structure, and hence

the ferroelectricity of the material. However, the polarization measurements on single crystals and dielectric measurements show that both spontaneous polarization and ferroelectric phase transition temperature increase with Li-concentration. Such an enhancement of ferroelectricity may be accounted for by the very strong ability of the off-centering of Li in perovskite[9]. Moving of Li toward an off-centering position then triggers the large local displacement of Ag along the same direction, leading to a ferroelectric state with large polarization in the ALN solid solutions. This inference is also supported by the Li-concentration dependence of rhombohedral distortion. As shown in Fig. 5, although the lattice constant  $a_r$  of rhombohedral cell remains nearly unchanged, however, the rhombohedral angle  $\alpha$  decreases monotonically with Li-concentration, indicating that increasing the Li-concentration enhances the rhombohedral distortion. As a result, we observed a linear increase in ferroelectric phase transition temperature and spontaneous polarization (Fig. 5(d)) with the rhombohedral angle  $\alpha$ .

## 4.2 Proposed phase diagram

On the basis of results described above, a phase diagram of ALN solution is summarized in Fig. 6, where T, O, R and M represent tetragonal, orthorhombic, rhombohedral, and monoclinic symmetries, respectively. At room temperature, structure transformation from O to R phase at  $x_c$  dramatically changes the polar nature of ALN. It consists of weak FE and strong AFE in O phase, but very strong FE in R phase. At higher temperature, successive phase transitions occur. The exact structures of high temperature phases remain to be clarified by further investigations using synchrotron radiation or neutron diffractions. However, the symmetry may be attributed qualitatively on the basis of the reports on  $\text{AgNbO}_3$  [16] and ALN [24, 25]. We notice that our phase diagram is basically in agreement with those of Nalbandyan et al. [24] and Sakabe et al. [25], but different from that of Wada et al.[26] who prepared the samples by a process starting from a heavily non-stoichiometric composition that might cause completely different phase evolution.

## 5 Summary

In summary, we have demonstrated that strong local polarization of Ag in  $\text{AgNbO}_3$  can be effectively induced into a ferroelectric state by chemically



modifying with Li substitution, which favors a rhombohedral distortion. In the rhombohedral phase, the ferroelectricity is derived from both atomic displacements of A- and B-site atoms in the perovskite structure. Furthermore, increasing Li-concentration enhances the rhombohedral distortion, consequently leading to the linear increase of ferroelectric phase transition and spontaneous polarization with Li-concentration.

**Acknowledgments** This work was partly supported by Collaborative Research Project of Materials and Structures Laboratory of Tokyo Institute of Technology, and Grant-in-Aid for Scientific Research, MEXT, Japan

## References

- [1] Lines M E and Glass A M 1977 *Principle and Application of Ferroelectrics and Related materials*, (Oxford: Clarendon Press, )
- [2] Jaffe B, Cook W R Jr and Jaffe H 1971 *Piezoelectric ceramics*, (London:Academic)
- [3] Scott J F 2000 *Ferroelectric memories*, (Berlin:Springer)
- [4] Fu D, Itoh M, Koshihara S, Kosugi T and Tsuneyuki S 2008 Phys. Rev. Lett. **100** 227601
- [5] Saito Y, Takao H, Tani T, Nonoyama T, Takatori K, Homma T, Nagaya T and Nakamura M 2004 Nature (London) **432** 84
- [6] Fu D, Itoh M and Koshihara S 2008 Appl. Phys. Lett. **93** 012904
- [7] Fu D, Itoh M and Koshihara S 2010 J. Phys.: Condens. Matter. **22** 052204
- [8] Tazaki R, Fu D, Itoh M, Daimon M and Koshihara S 2009 J. Phys.: Condens. Matter **21** 215903
- [9] Bilc D I and Singh D J 2006 Phys. Rev. Lett. **96** 147602
- [10] Grinberg I and Rappe A M 2004 Appl. Phys. Lett. **85** 1760
- [11] Cohen R E 1992 Nature (London) **358** 136
- [12] Egami T, Dmowski W, Akbas M and Davies P K 1998 in *First-principles Calculations for Ferroelectrics-Fifth Williamsburg Workshop*, edited by R. Cohen ( NY:American Institute of Physics),pp. 1-10
- [13] Kuroiwa Y et al. 2001 Phys. Rev. Lett. **87** 217601
- [14] Grinberg I and Rappe A M 2003 in *Fundamental Physics of Ferroelectrics 2003*, edited by P. K Davies and D. J. Singh ( NY: American Institute of Physics), pp. 130-138
- [15] Kato H,Kobayashi H and Kudo A 2002 J. Phys. Chem. B **106**, 12441

- [16] SciauPh, Kania A, Dkhil B, Suard E and Ratuszna A 2004 J. Phys.: Condens. Matter **16** 2795
- [17] Fu D, Endo M, Taniguchi H, Taniyama T and Itoh M 2007 Appl. Phys. Lett. **90** 252907
- [18] Francobe M H and Lewis G 1958 Acta Crystallogr. **11** 175
- [19] Fu D, Endo M, Taniguchi H, Taniyama T, Koshihara S and Itoh M 2008 Appl. Phys. Lett. **92** 172905
- [20] Fu D, Itoh M and Koshihara S 2009 J. Appl. Phys. **106** 104104
- [21] Levin I, Krayzman V, Woicik J C, Karapetrova J, Proffen T, Tucker M G and Reaney I M 2009 Phys. Rev. B **79** 104113
- [22] Pawelczyk M 1987 Phase Transitions **8** 273
- [23] Petzelt J, Kamba S, Buixareras E, Bovtun V, Zikmund Z, Kania A, Koukal V, Pokorny J, Polvka J, Pashkov V, Komandin G and Volkov A 1999 Ferroelectrics **223** 235
- [24] Nalbandyan V B, Medviediev B S, and Beliyev I N 1980 Izv. Akad. Nauk SSSR, Neorg. Mater. **16**, 1819 (1980).
- [25] Sakabe Y, Takeda T, Ogiso Y and Wada N 2001 Jpn. J. Appl. Phys., Part 1 **42** 5675
- [26] Wada S, Saito A, Hoshina T, Kakemoto H, Tsurumi T, Moriyoshi C and Kuroiwa Y 2006 Jpn. J. Appl. Phys., Part 1 **45** 7389
- [27] Kania A, Roleder K and Lukaszewski M 1984 Ferroelectrics **52** 265
- [28] Kania A and Kwapulinski J 1999 J. Phys.: Condens. Matter **11** 8933
- [29] *Ferroelectrics and Related Substances*, Landolt-Bornstein, New Series, Group III, Vol. 36, Pt. A1, edited by Y. Shiozaki, E. Nakamura, and T. Mitsui 2001 (Springer, Berlin)
- [30] C. A. P. de Araujo, J. D. Cuchiaro, L. D. McMillan, M. Scott and J. F. Scott 1995 Nature (London) **374**, 627

Table 1: Structural parameters obtained from Rietveld refinement for x=0.1.  
*Note:* The isotropic thermal parameters were kept at a value of  $0.5 \text{ \AA}^2$  in the refinements because we cannot find significant improvement of the refinement when changing these parameters.

Space group(No.)		R3c(161)		
$a/\text{\AA}$		5.52055(9)		
$b/\text{\AA}$		5.52055(9)		
$c/\text{\AA}$		13.7938(3)		
$\alpha$		90		
$\beta$		90		
$\gamma$		120		
volume/ $\text{\AA}^3$		364.07		
Atom	site	x	y	z
Ag/Li	6a	0	0	0.2545(8)
Nb	6a	0	0	0.0097(8)
O	18b	0.5533	1	0.2599(9)

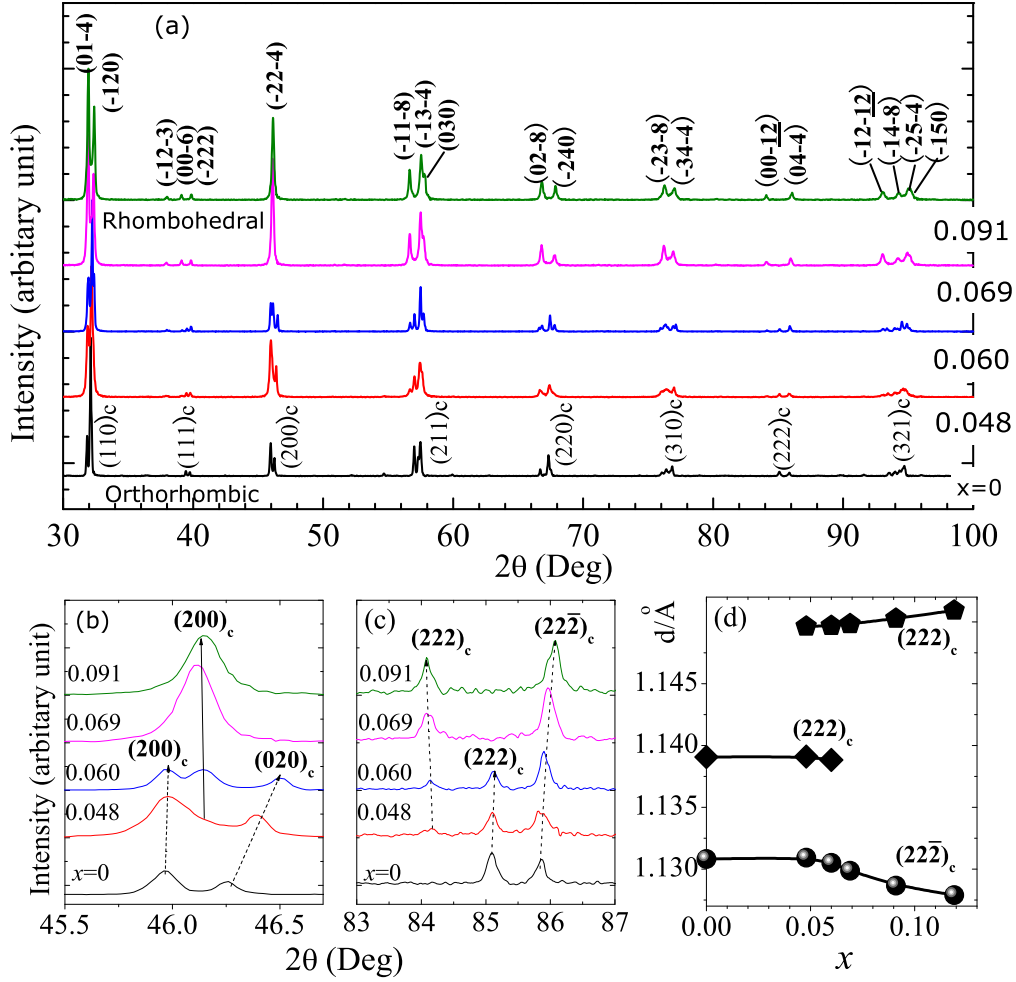


Figure 1: (a) Powder X-ray diffraction patterns of  $\text{Ag}_{1-x}\text{Li}_x\text{NbO}_3$  solid solutions. The major diffraction peaks are also indexed. For simplification, the plane indices of pseudocubic structure (indicated by a subscript of  $c$ ) are given for the mother material  $\text{AgNbO}_3$ . (b) and (c) show the enlarged views of the diffraction peaks of  $(200)_c$  and  $(222)_c$ , respectively. Structure change can be clearly seen from the splittings of these diffractions. (d)  $d$ -spacings vs concentration for the  $(222)_c$  planes.

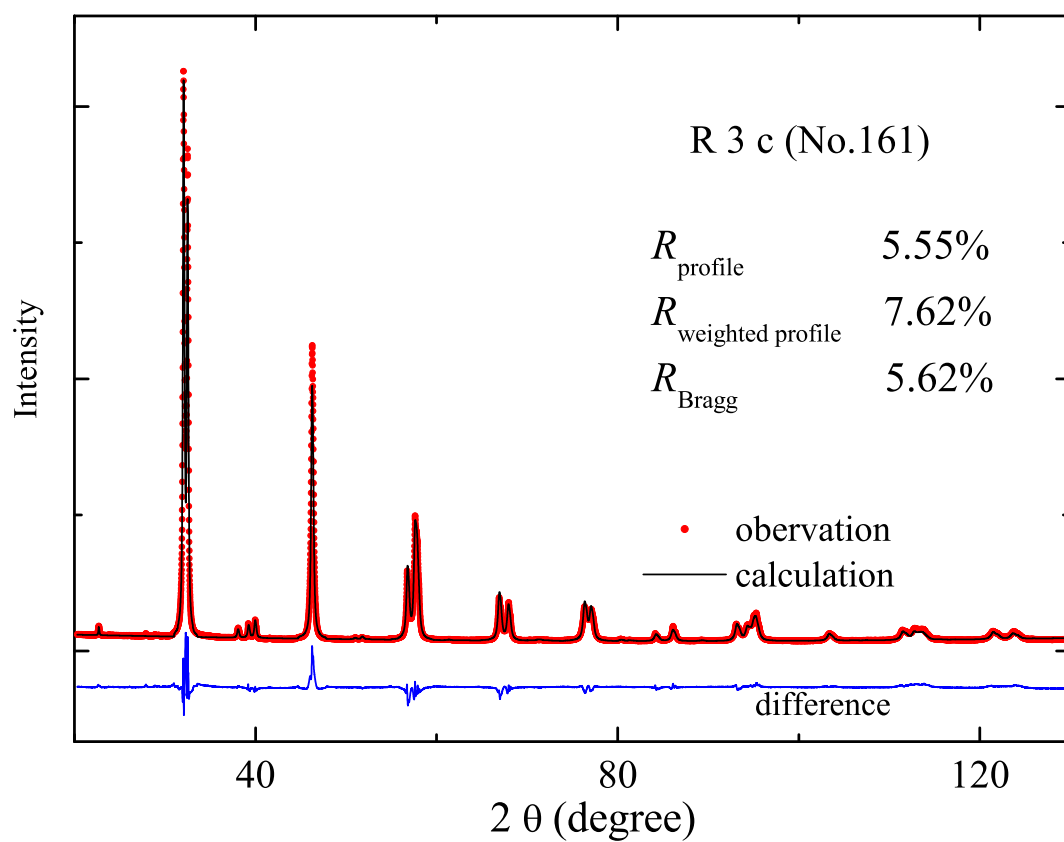


Figure 2: Observation, calculation and difference profiles for  $\text{Ag}_{1-x}\text{Li}_x\text{NbO}_3$  ( $x = 0.1$ ). Structural refinements at room temperature were performed with space group of  $R\bar{3}c$ (No.161).  $R$ -factors were given in the figure.

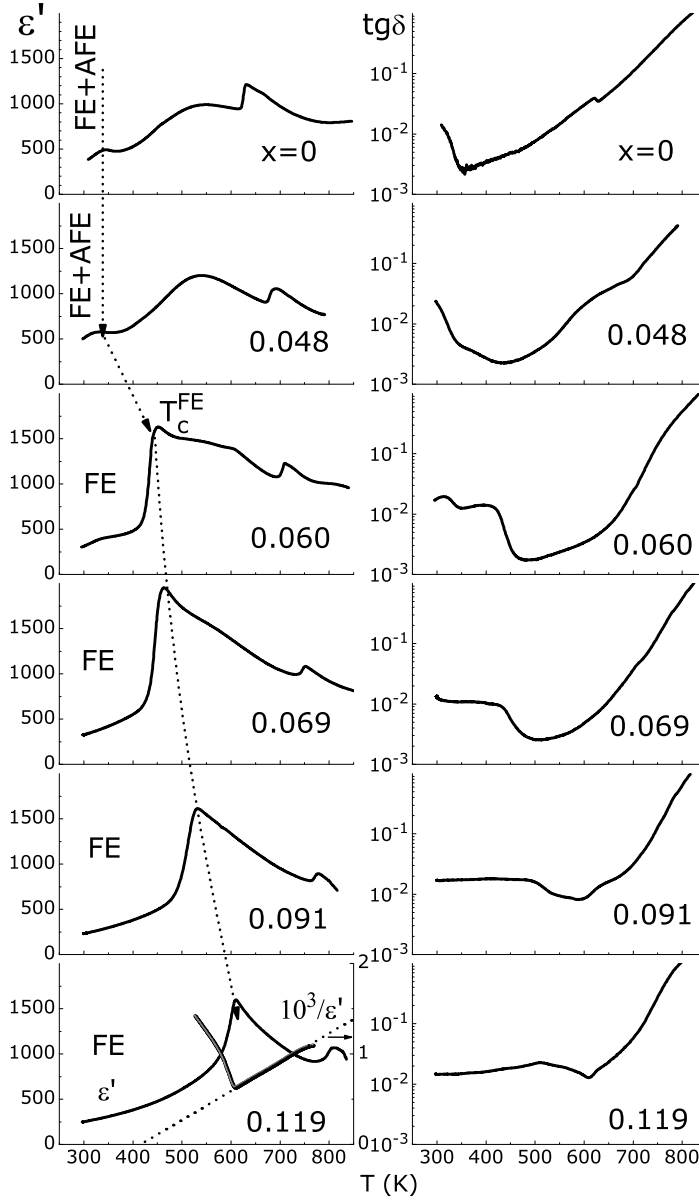


Figure 3: Temperature dependence of dielectric constant and loss. Data for  $x = 0$  are from Ref.[17]. Reverse dielectric constant is also given for the composition with  $x = 0.119$ .

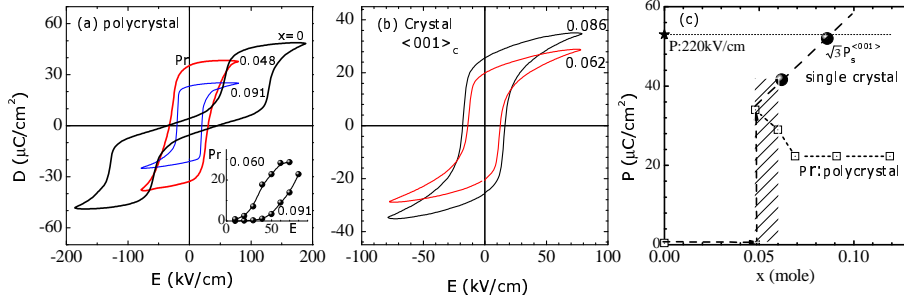


Figure 4:  $D - E$  hysteresis loops for (a) ceramics and (b)  $\langle 001 \rangle_c$ -oriented crystals. Inset shows the electric field dependence of  $P_r$  for ceramics with  $x = 0.060$  and  $0.091$ . (c) Composition dependence of remanent polarization (square) measured at  $80\text{kV}/\text{cm}$  for ceramics, and spontaneous polarization (black circle) of single crystals; Shaded region indicates the phase boundary between orthorhombic and rhombohedral structures; Star ( $\star$ ) and dash line indicate the polarization value obtained at  $220\text{ kV}/\text{cm}$  for  $\text{AgNbO}_3$  ceramics samples[17].



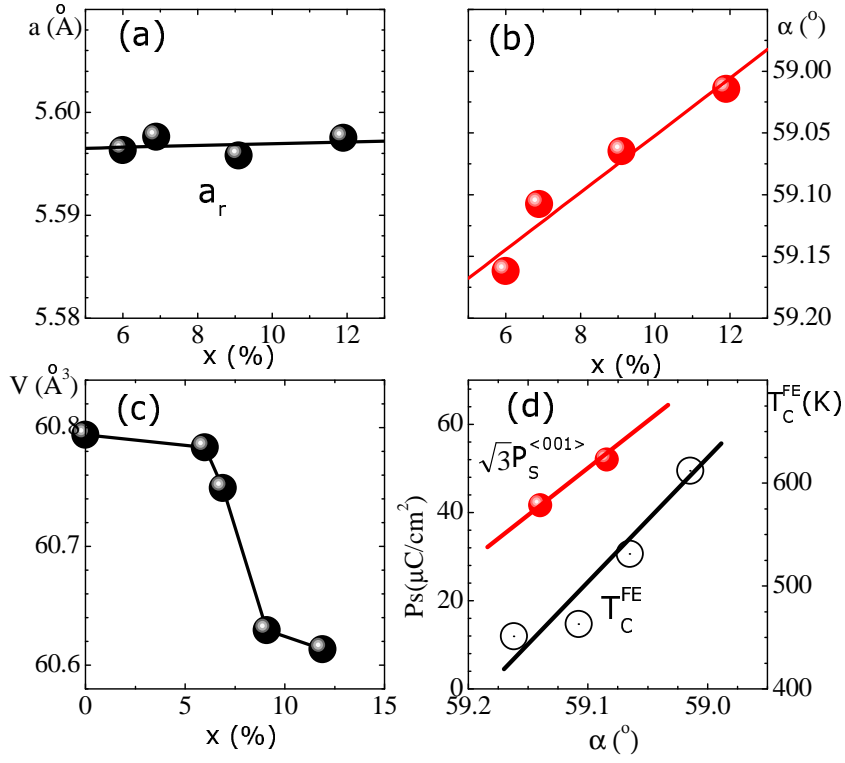


Figure 5: (a) Lattice constants of the rhombohedral cell for  $\text{Ag}_{1-x}\text{Li}_x\text{NbO}_3$  solid solutions. (b) Change in rhombohedral angle  $\alpha$ . (c) Change in volume of the perovskite cell. (d) Relationships of ferroelectric phase transition and spontaneous polarization with  $\alpha$ .

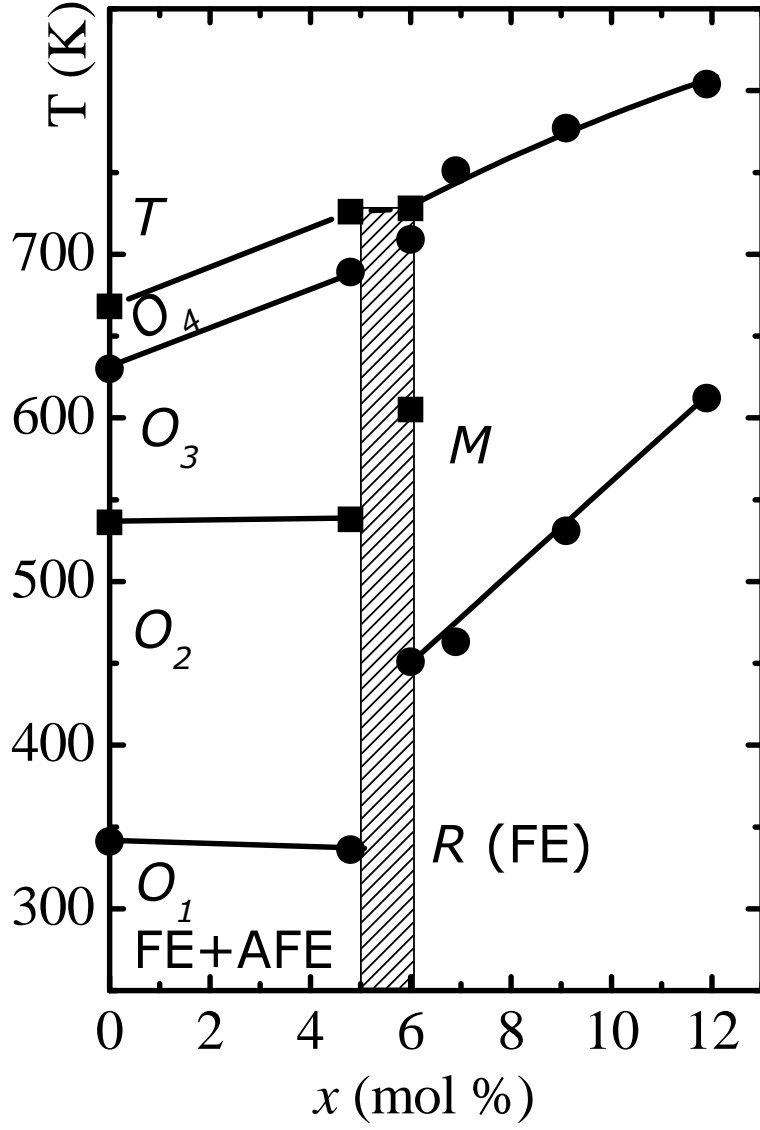


Figure 6: Phase diagram proposed for  $\text{Ag}_{1-x}\text{Li}_x\text{NbO}_3$  solid solution. Shaded area indicates the phase boundary. T, O, R, M indicate the tetragonal, orthorhombic, rhombohedral, and monoclinic structures, respectively.